Nanoscale Advances

ROYAL SOCIETY OF CHEMISTRY

PAPER

View Article Online
View Journal | View Issue

Cite this: *Nanoscale Adv.*, 2024, **6**, 2209

Self-standing bacterial cellulose-reinforced poly(3,4-ethylenedioxythiophene)/poly(4-styrenesulfonate) doped with graphene oxide composite electrodes for high-performance ionic electroactive soft actuators†

Yujiao Wu, * Qiyuan Cui, Ruibin Qi and Fan Wang*

Flexible electrode films with good film-forming properties, large deformation ability, high conductivity, and strong charge and discharge capabilities are crucial for ionic electroactive polymer soft actuators. However, there are still challenges in preparing high-quality electrode films that can combine well with the intermediate polyelectrolyte to form high-performance soft actuators. Herein, we propose an advanced sandwich ionic electroactive actuator utilizing self-standing bacterial cellulose (BC) reinforced poly(3,4-ethylenedioxythiophene)/poly(4-styrenesulfonate) (PP) doped with graphene oxide (GO) conductive composite electrodes and a Nafion ion-exchange membrane *via* a hot-pressing method. The prepared BC–PP–GO electrodes have good film-forming properties with a Young's modulus of 1360 MPa and a high conductivity of 150 S cm^{-1}. The hot-pressed BC–PP–GO/Nafion ionic actuator exhibited a large bending displacement of 6.2 mm (1 V, 0.1 Hz) with a long-term actuation stability up to 95% over 360 cycles without degradation. Furthermore, we introduced the actuator's potential applications including bionic grippers, flies, and fish, providing more opportunities for the development of next-generation micromanipulators and biomimetic microrobots in cm-scale space.

Received 5th February 2024
Accepted 11th March 2024

DOI: 10.1039/d4na00112e

rsc.li/nanoscale-advances

1. Introduction

Ionic electroactive polymers (IEAPs) are advanced smart materials that have garnered significant interest in the fields of soft microrobots, artificial muscles, and biomedical applications due to their unique ability to deform under electrical stimulation.[1–7] Specifically, smart cm-scale soft robots using IEAP materials possess bionic characteristics which are preferable to typical rigid actuators because of their flexibility, simple construction, miniaturization, safety, biocompatibility, and low energy consumption.[1,6,8–11] Typical IEAPs are ionic polymer metal composites (IPMCs), which are composed of a central ion-exchange polymer (*e.g.*, Nafion, Flemion, and Aciplex) and electroless plated metal electrodes (*e.g.*, Pd, Pt, Ag, and Au) on both sides.[9–17] Under an external electric field, the hydrated cations in Nafion flow towards the cathode through the ion nanochannels, causing the cathode side to swell and eventually bend toward the anode.

Although IPMC actuators have been developed for numerous applications (*e.g.*, bionic fin robots,[1] minimally invasive surgical tools,[6] biomimetic soft crawling robots,[18] manipulators,[19] and micropumps[20,21]), they still have specific disadvantages. The outer metal electrodes generated by multiple electroless plating generally have rough electrode surfaces and poor adhesion, which adversely affects IPMC charging. In addition, an IPMC's metal electrode is prone to damage and cracking over thousands of bending cycles, resulting in easy peeling, poor repeatability, and easy relaxation, which limit the actuation properties of IPMCs. Actually, flexible electrode films with excellent film-forming properties, large deformation abilities, high conductivity, and strong charge and discharge capabilities are crucial for improving the electromechanical properties of IPMC actuators. However, preparing high-quality electrode membranes that could work well with the intermediate electrolyte layer to develop high-performance ionic soft actuators remains a challenge.

Poly(3,4-ethylenedioxythiophene) (PEDOT)/poly(4-styrenesulfonate) (PSS) (denoted as PP) has been developed as a promising conductive polymer in recent decades owing to its high chemical and thermal stability, softness, and electrical conductivity.[22–24] Some researchers have adopted commercially available or doped-modified PP as an alternative electrode for preparing IEAP actuators, typically employing four preparation methods: drop-casting,[25–27] dip-casting,[28,29] spin-coating,[30–33] and hot-pressing.[7] However, the dip/drop-casting method causes differences in evaporation rates on the substrate or

School of Mechanical Engineering, Zhejiang Sci-Tech University, Hangzhou 310018, China. E-mail: wuyujiao@zstu.edu.cn; fwang@zstu.edu.cn

† Electronic supplementary information (ESI) available. See DOI: https://doi.org/10.1039/d4na00112e

concentration fluctuations, readily inducing uneven electrode surfaces. It is difficult to control the thickness of the PP electrode film by the spin-coating method at high speeds, and the excess solution is cast off the substrate, resulting in a significant waste of coating material. The hot-pressing method initially requires self-standing PP electrode films, yet commercially available PP has poor film-forming capabilities.

In order to obtain self-supporting and controllable PP electrode films, a reinforcing material is considered. Bacterial cellulose (BC) is an ideal natural green reinforcing material for fabricating a high-quality modified PP electrode film due to its unique dense reticulated nanostructure, hydrophilicity, biodegradability, and biocompatibility.[34,35] Recently, some BC-based ionic electroactive actuators exhibited bending deformations, such as BMIM-Cl-FDBC,[36] TOBC-IL-G,[37] FCBC-PPy-IL,[38] and BC-IL-MWCNT,[39] as well as our recently reported BC-IL-PVA[40] and CCNF-IL-GN actuators.[41] However, the majority focused on optimizing the intermediate polyelectrolyte layer, and then depositing PP solution on the polyelectrolyte surfaces *via* the dip/drop-casting method to obtain a three-layer actuator, which cannot guarantee the uniformity of the electrode films. Considering the current drawbacks, further development of high-quality PP electrode films and optimization of BC-based electroactive actuators are essential.

In the current study, we developed ultrathin free-standing BC-reinforced PP doped with graphene oxide (GO) conductive composite electrode membranes and then fabricated ionic electroactive soft actuators based on BC–PP–GO electrode films with a Nafion ion-exchange film *via* a hot-pressing method. Furthermore, we analyzed the prepared composite membranes' morphology, chemical structure, crystallinity, mechanical properties, and thermal stabilities. We also evaluated the actuation performances of the hot-pressed BC–PP–GO/Nafion actuators at various input sinusoidal voltages of 0.5–2.0 V and frequencies of 0.1–10 Hz. Additionally, the effect of GO doping in PP electrodes on the actuation properties was evaluated. Ultimately, the BC–PP–GO actuators' potential applications were demonstrated, including microgrippers, biomimetic flies, and fish, which provide more opportunities for the development of next-generation micromanipulators and biomimetic microrobots in cm-scale spaces.

2. Experimental section

2.1. Materials

PP solution (CLEVIOSTM F ET, solid content: 3.0–4.0%) from Heraeus was used as the conductive electrode material. Guilin Qihong Tech Co. Ltd. supplied bacterial cellulose (BC, 0.75 wt%

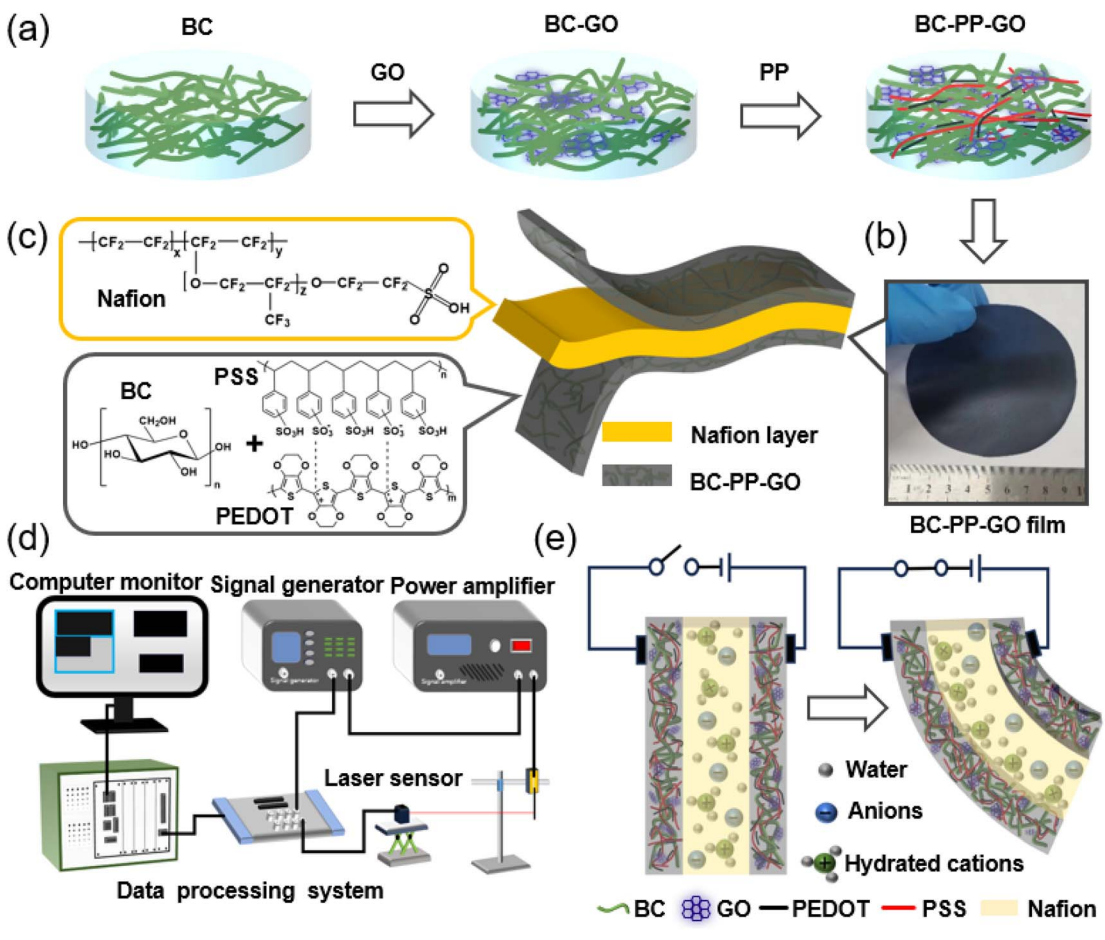

Fig. 1 Configuration of the BC–PP–GO/Nafion actuator: (a) diagram for BC–PP–GO electrode film preparation. (b) Image of a self-standing BC–PP–GO electrode film. (c) Chemical formulae of Nafion and BC–PP. (d) Actuation testing equipment. (e) Actuation principle.

aqueous dispersion) that was employed as a reinforcement. Single layer graphene oxide (GO, flake size: 0.5–5 μm, thickness: ~1 nm) was purchased from Suzhou Hengqiu Tech. Co., Ltd. An ion-exchange Nafion N212 film with a thickness of 50 μm was purchased from DoPont.

2.2. Preparation of a BC–PP–GO/Nafion actuator

In Fig. 1a, 10 g BC containing 20 g water and 0.01 g GO was stirred at 700 rpm for 1 h, and then added to 20 g PP solution with stirring for 6 h, followed by a 30 min degassing period. After this, the mixed BC–PP–GO dispersion (9 g) was poured into a 100 mm-diameter PTFE evaporating dish and heated (60 °C, 8 h) to form a self-supporting approx. 18 μm-thick BC–PP–GO electrode film (Fig. 1b). Two pieces of self-supporting electrode films sandwiched an ion-exchange Nafion-N212 film *via* a hot press (ST-15YP, Kunshan Lugong Precision Instrument Co., Ltd., China) with a pressure of 30 Mpa at 70 °C for 10 min to form a sandwich-structure BC–PP–GO/Nafion composite actuator with a thickness of approx. 80 μm (Fig. 1c).

2.3. Characterization

The conductivity, morphology, chemical interaction, crystallinity, tensile properties, and thermal stabilities of the prepared membranes were analyzed by using a ST2258C four-point method, a GeminiSEM 500 field emission scanning electron microscope (SEM, Carl Zeiss Co.), a Nicolet iS20 Fourier transform infrared spectroscope (FT-IR) with a wavenumber range of 500 to 4000 cm^{-1}, a D8 discover X-ray diffractometer (XRD, Bruker AXS Co.), a QT-6203A tensile tester, and a TG209F3 thermogravimetric analyzer (TGA, Netzsch Co.), respectively. The actuator's deformation sensing system (Fig. 1d) consists of a 33500B signal generator (Keysight Tech Co.), a FPA2000 power amplifier (Feel Tech Co.), an IL-300 laser displacement sensor (Keyence Co.), and a NI Pxle1078 data processing system (National Instruments Co.). Moreover, the bending strain ε is determined with the equation: $\varepsilon = 2dt/(d^2 + l^2)$, where d, t, and l stand for the peak displacement, thickness, and free length, respectively.

3. Results and discussion

3.1. SEM

The morphology of the BC-reinforced PP electrode film exhibits a comparatively homogeneous surface with a natural dense microfibrous structure of BC (Fig. 2a and b). After the addition of GO with nanopore structures, the BC–PP electrode surface shows well-dispersed GO without large aggregated particles

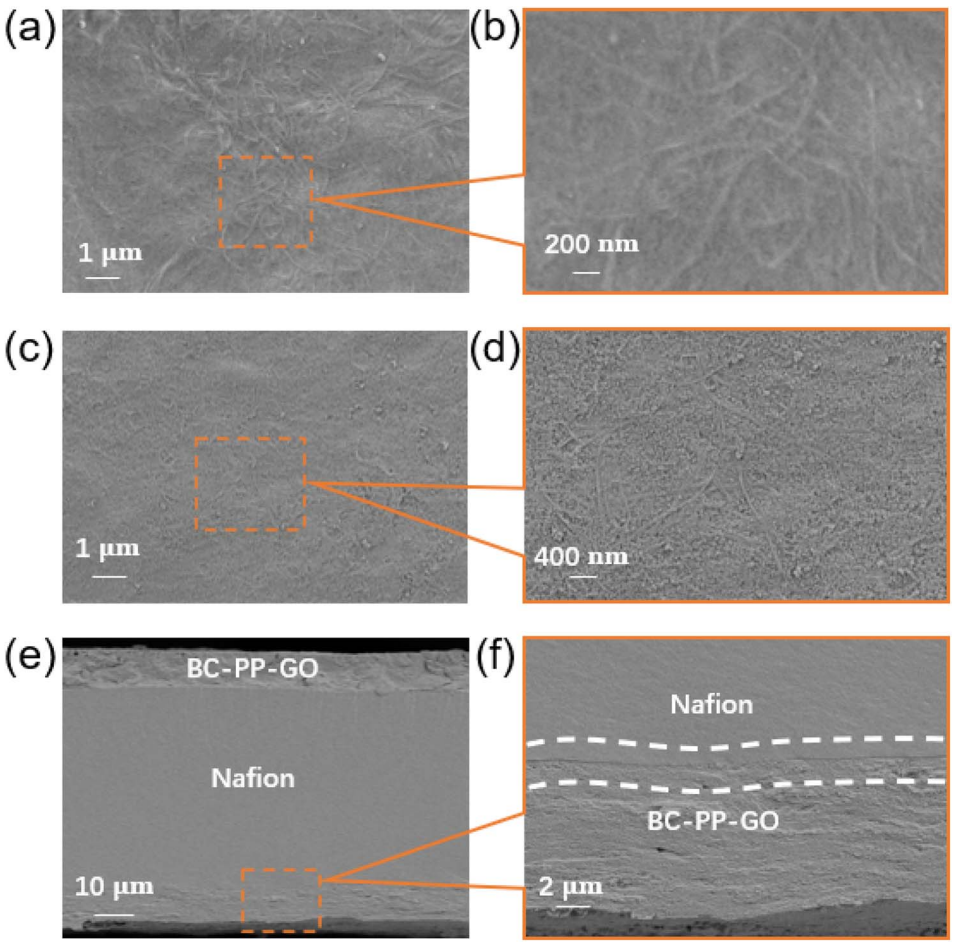

Fig. 2 SEM images of the (a and b) BC–PP film, (c and d) BC–PP–GO film, and (e and f) hot-pressed three-layer BC–PP–GO/Nafion actuator's cross-section.

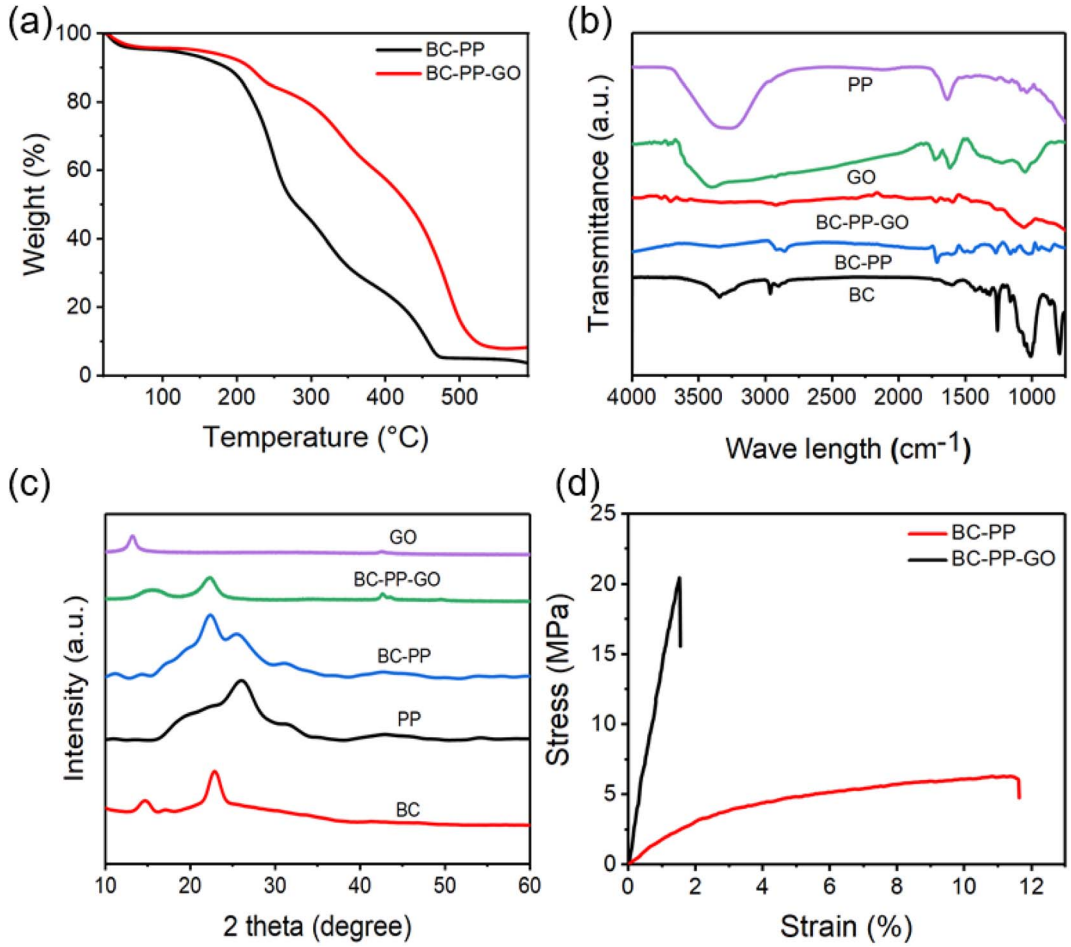

Fig. 3 (a) TGA curves, (b) FTIR spectra, (c) XRD patterns, and (d) tensile properties of the prepared BC–PP and BC–PP–GO composite films.

(Fig. 2c and d), providing the PP electrode with a larger accessible surface area for storing capacitive charge. Additionally, the hot-pressed BC–PP–GO/Nafion actuator's cross-section morphology has a sandwich composite structure (Fig. 2e and f). More crucially, the Nafion film attaches well to the BC-reinforced PP–GO electrode film without delamination. Notably, a densification interface layer exists as a result of mutual compression and solidification caused by applied pressure with heating. Furthermore, the porous dense microfibrous surfaces of the BC–PP–GO electrodes increase the contact area with the Nafion layer and enhance adhesion *via* a hot-pressing method. Here, the well-adhered contact interface contributes to enhancing the actuators' electromechanical characteristics.

3.2. TGA

The thermal stability of the obtained BC–PP and BC–PP–GO films was evaluated with TGA (Fig. 3a). The first significant drop in weight was due to water evaporation below 120 °C, while the second notable decrease in weight beyond 200 °C was associated with the polymer's decomposition. TGA confirmed that the hot-pressing temperature (70 °C, 10 min) and the BC–PP–GO film's preparation drying conditions (60 °C, 8 h) did not cause any detectable chemical degradation of the obtained actuator.

3.3. FTIR

FTIR analysis (Fig. 3b) shows the chemical structure of the obtained samples. The peaks of PP at 2960–3342, 1645, 1120, 1094, and 946 cm^{-1} are attributable to O–H & C–H stretching, C–C bonds in the thiophene ring, the SO_3H group of PSS, C–O–C bending vibrations, and C–S–C stretching vibrations, respectively.[42] The absorption peaks of BC are characteristic of cellulose Iα.[43–45] The observed peaks of the BC-reinforced PP film at 2850–2920 cm^{-1} are related to C–H stretching vibration, 1717 cm^{-1} attributed to C–O stretching, 1510 cm^{-1} attributed to aromatic symmetrical stretching due to C=C, 1250 cm^{-1} related to C–H–O, and 1020 cm^{-1} attributed to C–O–C stretching vibration. After adding GO, the BC–PP–GO composite exhibits new peaks at 3600–3800 cm^{-1} (C–OH vibration from phenol) and 1600–1800 cm^{-1} (C–OH from carboxyl and C=O from the carbonyl group), as well as a slight shift in the absorption peaks and a lower intensity in comparison to those in the spectra of pure PP, BC, and GO. These observations confirmed the GO doping in the BC–PP electrode with the formation of new bonds and interactions between PP, BC, and GO.

3.4. XRD

In Fig. 3c, XRD patterns of BC at $2\theta = 14.7°$, 16.6°, and 22.9° show the characteristic diffraction peaks with the (100), (010),

and (110) planes of cellulose Iα.[46] After the PP electrode was modified by adding BC, two main peaks at around 14.9° and 22.6° were observed, and the diffraction peak at $2\theta = 26.1°$ decreased in contrast to that of pure PP. Additionally, the diffraction peak of BC–PP doped with GO occurred at $2\theta = 42.3°$, indicating that GO somewhat enhanced the crystallinity of the BC–PP electrode due to the interaction and cross-linking of BC, GO, and PP.

3.5. Tensile test

The tensile test further confirmed that BC and GO significantly impacted the mechanical characteristics of PP (Fig. 3d). Young's modulus of BC–PP doped with GO is 1360 MPa, which is larger than that of BC–PP of 172.4 MPa. The high mechanical properties and good self-standing film-forming properties of PP composite electrodes are beneficial to the actuation deformation of the actuator.

3.6. Electromechanical characteristics

As shown in Fig. 4, the electromechanical characteristics of the prepared actuators were evaluated with different electrical inputs. Fig. 4a shows the effect of input sinusoidal voltages (0.5–2.0 V) on the actuation properties of the BC–PP–GO actuator. The bending displacement clearly increases as the applied voltage increases. Based on the actuation principle of a capacitor-type actuator (Fig. 1e), a higher voltage generates more charge on the electrodes, which in turn causes more hydrated cations in Nafion to flow toward the cathode, inducing more swelling and larger bending displacement. Fig. 4b shows the BC–PP–GO actuator's bending displacement increasing from 1.3 to 6.2 mm as the frequency drops from 5 to 0.1 Hz since a lower applied frequency gives more time for bending. Similar results are observed in Fig. 4c, and the peak displacements climb correspondingly as the applied voltages increase and frequencies drop, with the highest displacement of 9.4 mm recorded at 2.0 V, 0.1 Hz.

Furthermore, we evaluated the effects of GO doping in the BC–PP electrode on the actuation properties (Fig. 4d–f). The bending displacement and the initial deformation slope of the GO-doped actuator significantly increased compared to that without GO in response to 1.0 V, 0.1 Hz. Specifically, the peak displacement of BC–PP with a GO actuator is higher than that

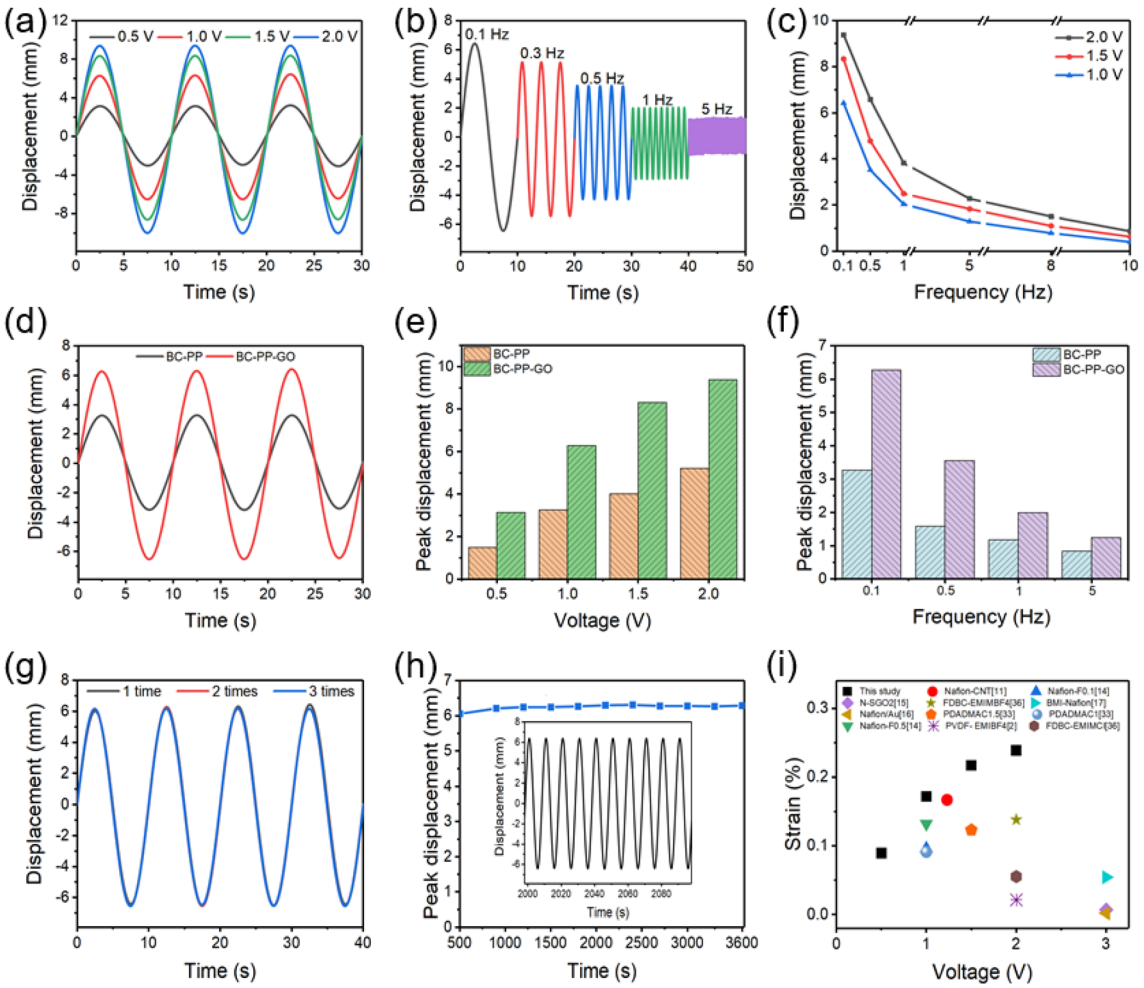

Fig. 4 Electromechanical actuation characteristics. (a) Bending curves of the BC–PP–GO actuator at various input voltages. (b) Bending curves at different applied frequencies. (c) Effect of different voltages and frequencies on the actuator peak displacement. (d–f) Actuation properties of BC–PP and BC–PP–GO actuators. (g) Reproducibility characteristics. (h) Actuation durability. (i) A comparison of the actuators' bending strain.

without GO under a given electric field, as illustrated in Fig. 4e and f. (*e.g.*, the GO-doped actuator exhibits a larger displacement of 6.2 mm compared to that without GO of 3.3 mm.), because the introduction of GO with high electrical conductivity somewhat improves the conductivity of the PP electrode. Here, the BC–PP film's conductivity of around 81 S cm^{-1} is improved to more than 150 S cm^{-1} by doping GO. Hence, the higher conductivity of the BC–PP–GO electrode improves the actuator's charging efficiency and capacity, further supporting Fig. 4d–f results that the GO-doped actuators increase conductivity and charging, thus facilitating the bending deflection of the actuator.

We also evaluated key parameters of the actuator's electromechanical repeatability and durability (Fig. 4g and h). Fig. 4g shows three sets of nearly identical actuation deformation with peak displacements of 6.2 ± 0.1 mm (1.0 V, 0.1 Hz), indicating that the designed actuator as high repeatability over several cycles. Moreover, the actuator's peak displacements at 1.0 V, 0.1 Hz are plotted as a function of the actuation time (Fig. 4h). The BC–PP–GO/Nafion actuator exhibits a 6.2 mm persistent peak displacement with a long-term cycling stability of 95% over 360 cycles without degradation. More importantly, Fig. 4i compares the BC–PP–GO/Nafion actuators' bending strain to that of the reported ionic actuators. The proposed actuator shows outstanding actuation characteristics with a greater bending strain of 0.23%, which is attributed to the BC–PP–GO electrodes' great film-forming ability, high electrical conductivity with stretchability, fast charging capability, and strong interfacial adhesion with Nafion.

4. Applications

Herein, the promising applications of the BC–PP–GO/Nafion actuators were introduced such as bionic grippers, biomimetic flies, and biomimetic fish tails. Fig. 5a describes an object (15 mg) which is grasped by a bionic gripper based on two prepared actuators (Movie S1, ESI†). Specifically, the gripper was first opened at +2.0 V and moved down, and the object was clamped at −2.0 V, and then lifted and removed from point "a" to point "b". Following this the gripper was lowered and released at +2.0 V, and finally left at point "b", which shows that the bionic small gripper could pick up and manipulate tiny objects in narrow space. Furthermore, the actuators were applied as a biomimetic fly using an actuator for flapping wings up and down by controlling the applied voltage (Fig. 5b, Movie S2, ESI†). More interestingly, a biomimetic fish tail based on the actuator was developed to achieve swaying left and right (Fig. 5c, Movie S3, ESI†). As a whole, the designed actuator exhibits enormous possibilities for realizing gripping and flapping actions of biomimetic grippers, fish, or insects in a cm-scale

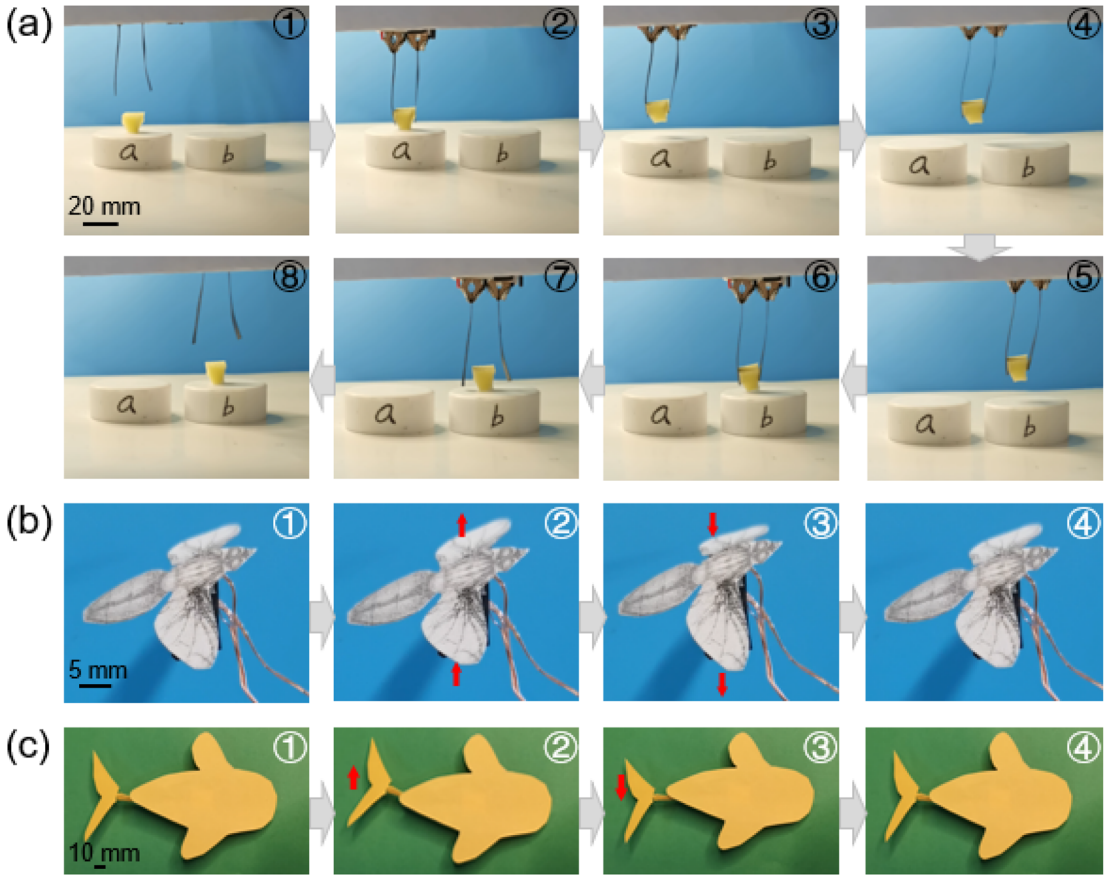

Fig. 5 Bionic applications of the prepared BC–PP–GO/Nafion actuator. (a) Biomimetic gripper utilizing two actuators for manipulating an object. (b) Simulation of a biomimetic fly flapping its wings up and down. (c) A biomimetic fish tail using an actuator.

space, which provides further opportunities for the development of next-generation actuators in micromanipulators and biomimetic microrobots.

5. Conclusions

Herein, we developed ultrathin free-standing BC-reinforced PP doped GO conductive composite electrode films with good film-forming properties (Young's modulus of 1360 MPa) and high conductivity (150 S cm^{-1}), and then fabricated a sandwich ionic electroactive soft actuator based on the BC–PP–GO electrodes and the ion-exchange Nafion membrane by a hot-pressing method. The obtained BC–PP–GO/Nafion ionic actuator exhibited a large bending displacement of 6.2 mm peak displacement (1.0 V, 10 Hz) with a long-term actuation stability up to 95% over 360 cycles without degradation due to the electrodes' great film-forming ability, high electrical conductivity with stretchability, fast charging capability, and strong interfacial adhesion. Furthermore, the potential actuator applications of bionic grippers, flies, and fish were introduced, which provides more opportunities for the next-generation development of micromanipulators and biomimetic microrobots.

Data availability

Data will be made available on reasonable request from the corresponding author.

Author contributions

Conceptualization: Yujiao Wu, Fan Wang; methodology: Yujiao Wu; formal analysis and investigation: Fan Wang; data curation and writing-original draft preparation: Qiyuan Cui, Ruibin Qi; writing – review and editing: Yujiao Wu, Fan Wang; funding acquisition: Yujiao Wu; resources and supervision: Fan Wang, Qiyuan Cui, Ruibin Qi.

Conflicts of interest

The authors declare that they have no known competing financial interests or personal relationships that could have appeared to influence the work reported in this paper.

Acknowledgements

This research was supported by the National Natural Science Foundation of China (52305327).

References

1 H. Wang, L. Yang, Y. Yang, D. Zhang and A. Tian, *Chem. Eng. J.*, 2023, **469**, 143976.
2 L. Lu, J. Liu, Y. Hu, Y. Zhang, H. Randriamahazaka and W. Chen, *Adv. Mater.*, 2012, **24**, 4317–4321.
3 H. Xu, C. Han, X. Liu, Z. Li, J. Liu and Z. Sun, *Sens. Actuators, A*, 2021, **332**, 113190.
4 C. Zhao, Y. Wang, G. Tang, J. Ru, Z. Zhu, B. Li, C. Guo, L. Li and D. Zhu, *Adv. Funct. Mater.*, 2022, **32**, 2110417.
5 Z. Xu, B. Zhu, X. Liu, T. Lan, Y. Huang, Y. Zhang and D. Wu, *Chem. Eng. J.*, 2023, **477**, 147246.
6 P. Rinne, I. Põldsalu, V. Zadin, U. Johanson, T. Tamm, K. Esko, A. Punning, D. Ende and A. Aabloo, *Sci. Rep.*, 2022, **12**, 21589.
7 Y. Bae, M. Park, M. Kim, S. H wang, S. Kim and M. Jeon, *Thin Solid Films*, 2020, **698**, 136848.
8 I. Apsite, S. Salehi and L. Ionov, *Chem. Rev.*, 2022, **1**, 1349–1415.
9 C. Zhao, Y. Ji, G. Tang, X. Zhao, D. Mei, J. Ru, D. Zhu and Y. Wang, *Polymers*, 2023, **3**, 733.
10 S. Lee, Y. Choi, J. Lee, T. Yang, J. Jho and J. Park, *J. Ind. Eng. Chem.*, 2023, **122**, 79–89.
11 T. Horiuchi, Y. Kato and T. Sugino, *Sens. Actuators, A*, 2023, **352**, 114178.
12 T. Ikeda, *Sci. Rep.*, 2023, **13**, 16669.
13 C. He, Y. Gu, J. Zhang, L. Ma, M. Yan, Y. Mou and Y. Ren, *Int. J. Mol. Sci.*, 2022, **7**, 3522.
14 J. Jung, S. Vadahanambi and I. Oh, *Compos. Sci. Technol.*, 2010, **4**, 584–592.
15 L. Naji, M. Safari and S. Moaven, *Carbon*, 2016, **100**, 243.
16 O. Yilmaz, I. Sen, B. Gurses, O. Ozdemir, L. Cetin, M. Sarikanat, Y. Seki, K. Sever and E. Altinkaya, *Composites, Part B*, 2019, **165**, 747.
17 I. Chen, P. Cottinet, S. Tsai, B. Foster, R. Liang, B. Wang and C. Zhang, *Sens. Actuators, B*, 2012, **515**, 171–172.
18 J. Carrico, T. Hermans, K. Kim and K. Leang, *Sci. Rep.*, 2019, **9**, 17482.
19 R. Jain, S. Majumder and A. Dutta, *Robot. Auton. Syst.*, 2013, **61**, 297–311.
20 T. Nguyen, N. Goo, V. Nguyen, Y. Yoo and S. Park, *Sens. Actuators, A*, 2008, **141**, 640–648.
21 S. Lee and K. Kim, *Smart Mater. Struct.*, 2006, **15**, 1103.
22 J. Li, J. Cao, B. Lu and G. Gu, *Nat. Rev. Mater.*, 2023, **8**, 604–622.
23 S. Kim, C. Kim, Y. Kim, N. Kim, W. Lee, E. Lee, D. Kim, S. Park, K. Lee, J. Rivnay and M. Yoon, *Nat. Commun.*, 2018, **9**, 3858.
24 Y. Xia and S. Dai, *J. Mater. Sci.*, 2021, **32**, 12746–12757.
25 S. Umrao, R. Tabassian, J. Kim, V. Nguyen, Q. Zhou, S. Nam and I. Oh, *Sci. Robot.*, 2019, **33**, 7797.
26 F. Yu, H. Ciou, S. Chen, W. Poh, J. Chen, J. Chen, K. Haruethai, J. Lv, D. Gao and P. Lee, *Nat. Commun.*, 2022, **13**, 390.
27 Y. Li, W. Liu, X. Gao, T. Zou, P. Deng, J. Zhao, T. Zhang, Y. Chen, L. He, L. Shao, Z. Yan and X. Zhang, *Sens. Actuators, A*, 2023, **354**, 114277.
28 F. Wang, L. Wang, Z. Wu and W. Wang, *J. Mater. Sci.*, 2023, **58**, 466–477.
29 F. Wang, Y. Kong and F. Shen, *Composites, Part B*, 2022, **228**, 109436.
30 M. Park, J. Kim, H. Song, S. Kim and M. Jeon, *Sensors*, 2018, **9**, 3126.

31 T. Nguyen, K. Rohtlaid, C. Plesse, G. Nguyen, C. Soyer, S. Grondel, E. Cattan, J. Madden and F. Vidal, *Electrochim. Acta*, 2018, **265**, 670–680.
32 Y. Liu, X. Sun, C. Lv and H. Xia, *Smart Mater. Struct.*, 2021, **30**, 125014.
33 Y. Wu, H. Minamikawa, T. Nakazumi and Y. Hara, *J. Oleo Sci.*, 2020, **69**, 1331–1337.
34 D. Gregory, L. Tripathi, A. Fricker, E. Asare, I. Orlando, V. Raghavendran and I. Roy, *Mater. Sci. Eng., R*, 2021, **145**, 100623.
35 J. Muiruri, J. Yeo, Q. Zhu, E. Ye, X. Loh and Z. Li, *Eur. Polym. J.*, 2023, **199**, 112446.
36 S. Kim, J. Jeon, C. Kee and I. Oh, *Smart Mater. Struct.*, 2013, **22**, 085026.
37 S. Kim, J. Jeon, H. Kim, C. Kee and I. Oh, *Adv. Funct. Mater.*, 2015, **25**, 3560–3570.
38 F. Wang, Q. Li, J. Park, S. Zheng and E. Choi, *Adv. Funct. Mater.*, 2021, **31**, 2007749.
39 Y. Wang, F. Wang, Y. Kong, L. Wang and Q. Li, *Smart Mater. Struct.*, 2022, **31**, 025023.
40 F. Wang, D. Huang, Y. Wu and D. Wang, *J. Mater. Sci.: Mater. Electron.*, 2023, **34**, 123.
41 F. Wang, D. Huang, Q. Li, Y. Wu, B. Yan, Z. Wu and S. Park, *Compos. Sci. Technol.*, 2023, **231**, 109845.
42 H. Du, M. Zhang, K. Liu, M. Parit, Z. Jiang, X. Zhang, B. Li and C. Si, *Chem. Eng. J.*, 2022, **428**, 131994.
43 Q. Li, R. Tang, H. Zhou, X. Hu and S. Zhang, *Carbohydr. Polym.*, 2023, **311**, 120754.
44 X. Liu, L. Cao, S. Wang, L. Huang, Y. Zhang, M. Tian, X. Li and J. Zhang, *Sci. Rep.*, 2023, **13**, 16024.
45 S. Srivastava and G. Mathur, *Biologia*, 2022, **77**, 3657–3668.
46 A. French, *Cellulose*, 2014, **21**, 885–896.